Electron Velocity Enhancement in Polarization-doped AlGaN

Linas ARDARAVIČIUS *, Oleg KIPRIJANOVIČ, Juozapas LIBERIS

Semiconductor Physics Institute, Center for Physical Sciences and Technology,
A. Goštauto 11, LT-01108 Vilnius, Lithuania

Three-dimensional electron gas/slabs (3DEG/S) can be obtained using the technique of 3-dimensional polarization-doping in graded AlGaN semiconductor layer on GaN. Transport characteristics of the graded AlGaN are investigated experimentally by means of nanosecond-pulsed measurements. The measured current-voltage dependences were used to determine drift velocity data assuming no change in electron density upon applied electric field. The velocity results are compared with that of GaN and ungraded AlGaN/GaN. Also, the experimental results are compared with those of Monte Carlo simulation.

Keywords: graded $Al_xGa_{1-x}N$/GaN, current-voltage dependence, polarization doping, strong electric fields, electron drift velocity.

1. INTRODUCTION

III-nitride semiconductors offer superior physical properties such as large bandgap, large breakdown field, and a strong piezoelectric and spontaneous polarization. To change electronic properties, besides conventional way such as doping with impurities, three-dimensional electron gas/slabs (3DEG/S) [1] or hole gas/slabs (3DHG/S) [2] can be obtained using the technique of polarization bulk doping in graded $Al_xGa_{1-x}N$ semiconductor layer.

In particular, ternary wurtzite graded AlGaN [3] is becoming of increasing importance in many semiconductor electronic [4–8] and optoelectronic device applications [9]. A graded AlGaN back-barrier design reduces the drain modulation caused by the negative-polarization interface and improves electron mobility in ultrathin (5 nm) channels, which helps to achieve greatly improved peak drive current and peak transconductance [8]. Recently, it was revealed that the polarization-doped light emitting diode (LED) has the improved electroluminescence intensity and external quantum efficiency compared with the conventional LED [9]. Crack-free GaN epitaxial layer was obtained after inserting 80 nm graded AlGaN buffer layer between GaN epilayer and high temperature AlN buffer [10]. Also, it was found that the insertion of a graded AlGaN layer between the GaN layer and the AlN buffer can change the signs of strain [11].

In this work the electric characteristics of the graded AlGaN are investigated experimentally at room temperature through nanosecond-pulsed measurements of electron drift velocity. Experimental results are compared with those of GaN and ungraded AlGaN/GaN, and with Monte Carlo simulation data in $Al_{0.2}Ga_{0.8}N$. .

2. SAMPLES

The investigated $Al_xGa_{1-x}N$/GaN structures (Fig. 1) were grown on c-plane sapphire by metal-organic chemical

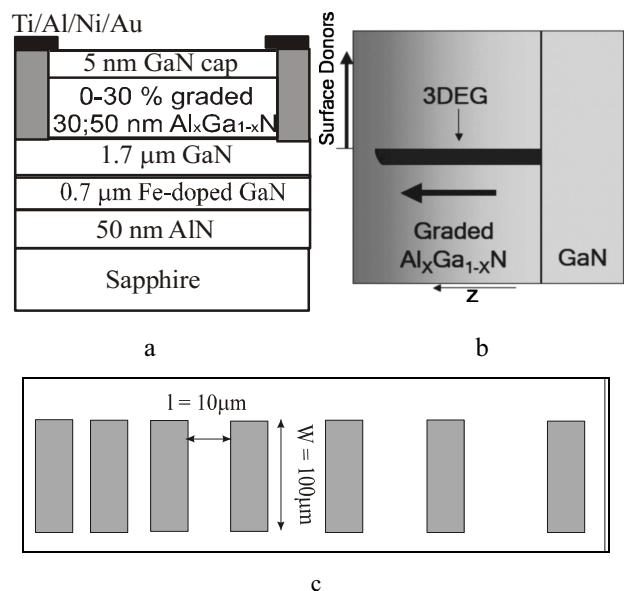vapor deposition (MOCVD) at the University of Califormia, Santa Barbara (Fig, 1, a).

a   b

c

Fig. 1. A schematic view of an $Al_xGa_{1-x}N$/GaN structure with deposited Ti/Al/Ni/Au ohmic contacts (a); 3DEG/S in an AlGaN layer (b); the investigated sample (channel width w = 100 μm, length l = 10 μm) in a TLM pattern (c)

The growth was initiated by a 50 nm thick AlN layer followed by a Fe-doped 0.7 μm GaN and 1.7 μm GaN buffer layer. Then a graded AlGaN layer was deposited. The alloy composition x as well as polarization was varied continuously from the GaN layer through a region of AlGaN material, and the fixed polarization charge was spread over the distance of the grading length. Polarization grading (doping) enables 3DEG/S (Fig. 1, b) with advantages of modulation doping – absence of carrier freeze-out and impurity scattering. Finally, the structure is capped by a GaN layer to improve the ohmic contacts. For the ohmic contacts, a Ti/Al/Ni/Au multilayer was annealed for 30 s at 870 °C in a N_2 atmosphere. The mesa isolation

---
*Corresponding author: ph.: +370-5-2618101; fax: +370-5-2627123.
E-mail: *linas.ardaravicius@ftmc.lt* (L. Ardaravičius)

was done with chlorine-based dry etch. Samples (width $w = 100$ μm, length $l = 10$ μm) to measure the electric characteristics were taken from transfer length model (TLM) patterns (Fig. 1, c) processed with standard lift-off technique.
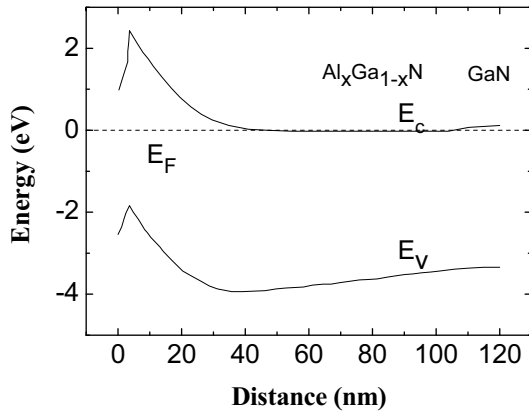

Fig. 2. Calculated zero bias band diagram of the graded over 100 nm $Al_xGa_{1-x}N$/GaN assuming a 0.9 eV Schottky barrier for the metal–GaN junction [4, 12].

Zero bias band diagram was calculated according to [12] (see Fig. 2) in order to show electron distribution place over the Fermi (E_F) level in the conduction band (E_c) [4].

When grading distance was 100 nm the 3DEG/S was spread within 70 nm; for shorter distances such as 50 nm and 30 nm 3DEG/S was distributed within 29.5 nm 18.5 nm, respectively (see also [1]).

The electron density n was determined by means of capacitance-voltage measurements and the mobility μ was calculated using an expression $\mu = l / (R\,e\,n\,w)$, where R is the sample resistance, e is the electron charge.

The dominant scattering mechanisms limiting electron mobility at room temperature and low electric field were alloy scattering and optical phonon scattering. Alloy scattering is reduced when grading distance increases [1].

Low-field transport properties of the investigated structures are presented in Table 1.

Table 1. Low-field transport properties in graded $Al_xGa_{1-x}N$/GaN

Grading lenght, nm	Electron density	Electron mobility, cm^2/(V·s)
30	5×10^{18} cm^{-3}, 1.29×10^{13} cm^{-2}	554
50	3×10^{18} cm^{-3}, 1.3×10^{13} cm^{-2}	675

3. EXPERIMENTAL

The *I-V* dependences were measured by means of the nanosecond-pulsed technique. A standard pulse generator was used to produce electrical pulses in a 50 Ω transmission line, with the amplitude up to 25 V and duration t of 100 ns – 500 ns. Shorter high-voltage nanosecond pulses ($t = 1$ ns – 40 ns) were generated using a generator based on discharge in coaxial line circuit by

means of mercury-wetted relay. These shorter pulses were used in order to minimize a local increase in crystal temperature due to dissipated Joule electric power, i. e. so called self-heating effect, since the carrier mobility is dependent on both the electric field strength and the lattice temperature.

Schematic diagram of the experimental set-up is presented in Fig. 3. The set-up consists of the mercury-wetted relay generator (3) with a power supply (1) and a charged line (2). A generated electrical pulse with the duration depending on the charged line (2) length, is transmitted to the oscilloscope (15) through a delay line (5), a power attenuator with regulated attenuation (6), a switch (7), a gauge resistor (10) or the investigated sample (12), and fixed attenuators (13). The sample is placed in a thermostat (11). DC and temperature regimes of the sample are controlled by a digital multimeter (9) with the usage of bias tees (8). The signal is received by a two-channel digital oscilloscope of $0 - 125$ MHz bandwidth (15) and then directed to the computer monitor (16).
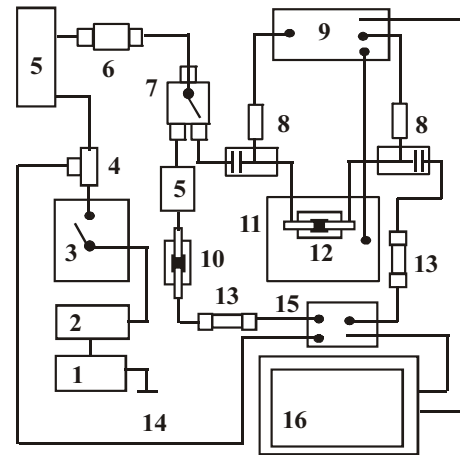

Fig. 3. Schematic diagram of the experimental set-up. 1 – power supply; 2 – charged line with a charged resistor; 3 – mercury-wetted relay generator; 4 – synchronization tee; 5 – delay line; 6 – tunable power attenuator; 7 – broadband switch; 8 – bias tee; 9 – digital multimeter; 10 – gauge resistor; 11 – cryo- or thermostat with a thermosensor; 12 – sample; 13 – broadband attenuator; 14 – synchronization channel; 15 – digital oscilloscope, 16 – computer monitor

Additionally, such oscilloscope enables to investigate the sample resistance dynamics for the pulses longer than 20 ns. As the result a family of *I-V* dependences each corresponding to time moments of spaced out pulse can be obtained.

Both sample and the high-frequency gauge resistor are mounted in the microstrip line holders. The holder consists of a metallic substrate, a high frequency dielectric plate and two coaxial-microsrip line adaptors used to connect with cables. The substrate serves as a ground conductor and has a 2 nm thick dielectric plate placed on it, with the dielectric permittivity $\varepsilon = 10$. The plate supporting line is 2 mm in width. The sample is connected to the line by Au microwires attached by thermocompression. Fig. 4 demonstrates a common view of the holder with the gauge resistor in the break of the line.
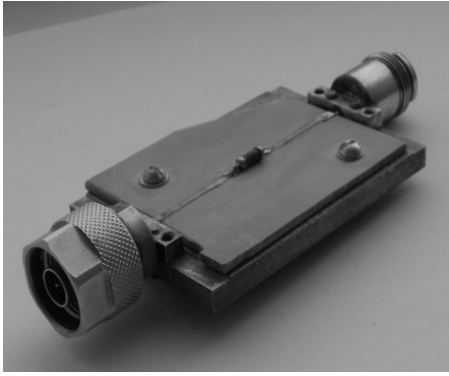
Fig. 4. Common view of a microstrip holder with two adaptors. Microstrip line is on a dielectric plate ($\varepsilon = 10$). The plate dimensions are $7{\times}5{\times}2$ cm^3. A high frequency gauge resistor placed into a break of the microstrip line

To obtain any value of the current-voltage dependence plot two measurements are required. A falling pulse amplitude is taken in the first measurement and the amplitude of a pulse transmitted through the sample is taken in another. The direct falling pulse amplitude measurement with a sufficient accuracy requires to take into account the complex equivalent circuit [13]. In our measurements, the falling pulse amplitude is found from the measurement of a pulse amplitude transmitted through the gauge resistor of known value. Such measurement modification allows one to use a simple equivalent circuit consisting of three resistors connected in series. These are an internal 50 Ω resistor of the generator (3), an unknown resistance of the sample and a 50 Ω input the oscilloscope resistor. Therefore, first input of the oscilloscope (16) receives a signal transmitted through the sample (12). The second input receives a signal transmitted through the gauge resistor (10). The coaxial switch (7) was used for commutation of these two measurements (see Fig. 3).

For the pulses shorter than 20 ns the broadband sampling or real time two-channel oscilloscopes of $0-5$ GHz bandwidth were used, as it was described in [14]. Current-voltage measurements were performed at room temperature up to 140 kV/cm electric fields.

The error of the pulse amplitude measurements with the use of the oscilloscopes is 4 %. The usage of the digital oscilloscope minimizes the error that appears due to lack of coincidence in time in these two measurements. However, an error induced by signal attenuation remains. At high applied electric field, the attenuation increases, and thus the error can reach up to 8 %.

4. EXPERIMENTAL RESULTS

Figure 5 presents measured current values as a function of applied electric field up to 60 kV/cm for 1 ns voltages pulses and up to 20 kV/cm for 500 ns pulses. The measured current values did not exceed 0.2 A for shorter pulses and 0.12 A for longer pulses. It is known that Joule heat is dissipated in the channel when the current passes through it. As a result, the current becomes reduced.

The longer the pulse width, the more heat is dissipated and the stronger is the current reduction [15]. For shorter pulses, in our experiment the effect of Joule heat on the

current is minimized 1.16 times at 18 kV/cm as the applied voltage pulse width was reduced from 500 ns down to 1 ns. Indeed, the current values at this particular field are 16 % higher for shorter pulses (Fig. 5).
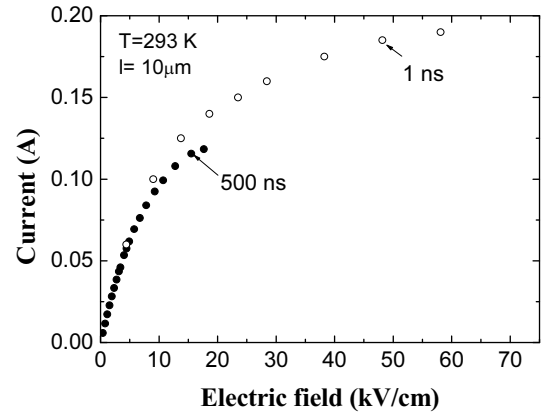

Fig. 5. Current-voltage characteristics for graded $Al_xGa_{1-x}N$/GaN channel at room temperature. Voltage pulse duration 500 ns and 1 ns

The drift velocity in graded $Al_xGa_{1-x}N$/GaN channel was estimated according to the expression $v_{dr} = I/(enw)$, where I was the current (pulse duration 4 ns) passing through the sample, assuming constant electron density upon applied electric field.

The electron drift velocity in graded $Al_xGa_{1-x}N$/GaN having longer (shorter) grading length (Fig. 6) was measured at room temperature at electric fields up to 140 kV/cm. The velocity is lower in graded $Al_xGa_{1-x}N$/GaN with shorter grading length. For comparison with the experimental data, ensemble Monte Carlo calculation results were taken from [16]. Up to now, the simulation using only fixed Al molar fraction of $x = 0.2$ of ternary $Al_xGa_{1-x}N$ was performed. The scattering mechanisms included into the simulation were alloy, ionized impurity, acoustic, and optical phonon scattering. Alloy scattering strength was defined by alloy scattering potential U_0 which varied from 0 eV to 2.7 eV.
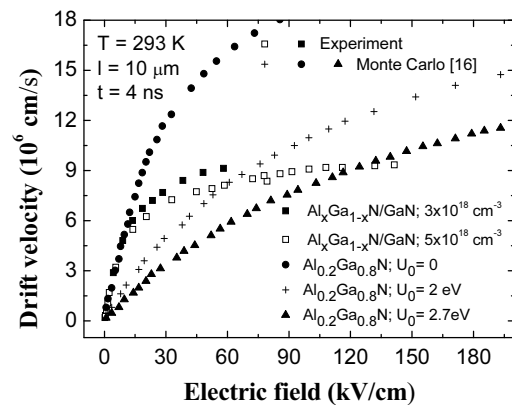

Fig. 6. Calculated [16] and measured drift velocity as a function of electric field for $Al_{0.2}Ga_{0.8}N$ and graded $Al_xGa_{1-x}N$/GaN, respectively. Different alloy scattering potential values U_0 are used in Monte Carlo procedure. Electron density used in the calculations is 10^{17} cm^{-3}

The calculated drift velocity results were similar with the experimental data up to 20 kV/cm only when there was no alloy scattering. The discrepancy, besides the lack of calculation with linear increase of Al composition, may also be caused by other scattering mechanisms not taken into account during simulation.

The electron drift velocity in graded $Al_xGa_{1-x}N/GaN$ having shorter grading length is comparable with that of AlGaN/GaN on GaN (Fig. 7). It also exceeds the velocity of GaN [17] below 35 kV/cm because there is no ionized impurity scattering, and it is lower that of AlGaN/GaN on Al_2O_5 [18] (sapphire) at electric fields exceeding 10 kV/cm.
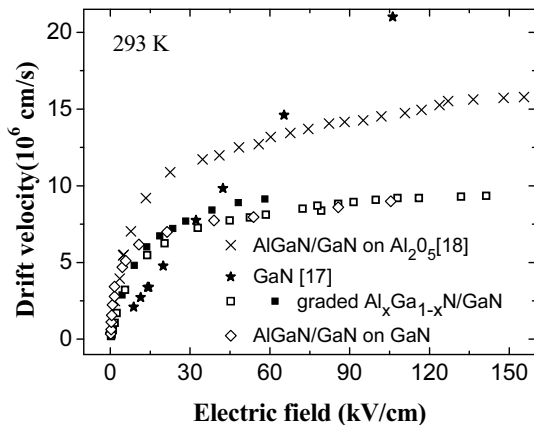

Fig. 7. Experimental drift velocity as a function of electric field in (un) graded AlGaN/GaN and bulk GaN channels

5. DISCUSSION

When comparing two graded channels, the drift velocity is higher in the channel with longer grading length (50 nm) (Fig. 6) since the electron mobility in it is affected by lower alloy scattering. Also, in nitride materials, there is a substantial difference between characteristic times for optical-phonon emission and their decay; this results in a significant accumulation of the launched LO phonons, i. e. non-equilibrium (hot) phonons. Hot phonons affect electron transport, namely, drift velocity. It is known that at a given electron density the drift velocity is higher if hot-phonon decay time is shorter [19]. In our case, we have two graded channels with different three-dimensional electron densities. According to optical experimental findings on bulk GaN the phonon decay time increases as density decreases [20]. Hence, it is reasonable to assume that a similar scenario is valid for AlGaN. This supports a statement that hot-phonon effect on drift velocity is weaker for the channel with lower electron density [see also, 17]. Consequently, the velocity is higher for the channel where grading length is longer. The velocity of both graded channels above 35 kV/cm is lower than that of GaN because of presence of alloy scattering and hot-phonon scattering.

6. CONCLUSIONS

In conclusion, we measured *I-V* dependences of graded AlGaN alloys at room temperature up to high electric fields. Using this data together with determined electron

density values we were able to estimate electron drift velocity. The velocity is enhanced compared with that of bulk GaN up to moderate electric fields. The results are interpreted in terms of alloy and non-equilibrium LO phonon scattering.

REFERENCES

1. **Rajan, S., DenBaars, S. P., Mishra, U. K., Xing, H. Grace, Jena, D.** Electron Mobility in Graded AlGaN Alloys *Applied Physics Letters* 88 (24) 2006: p. 042103; **Simon, J., Wang, A. K., Xing, H., Rajan, S., Jena, D.** Carrier Transport and Confinement in Polarization-induced Three-dimensional Electron Slabs: Importance of Alloy Scattering in AlGaN *Applied Physics Letters* 88 (24) 2006: p. 042109.
   http://dx.doi.org/10.1063/1.2165190

2. **Simon, J., Protasenko, V., Lian, C., Xing, H., Jena, D.** Polarization-induced Hole Doping in Wide-band-gap Uniaxial Semiconductor Heterostructures *Science* 327 (5961) 2010: pp. 60 – 64.
   http://dx.doi.org/10.1063/1.2168253

3. **Wei, Q., Wu, Z., Sun, K., Ponce, F. A., Hertkorn, J., Scholz, F.** Evidence of Two-Dimensional Hole Gas in p-Type AlGaN/AlN/GaN Heterostructures *Applied Physics Express* 2 (12) 2009: p. 121001.
   http://dx.doi.org/10.1143/APEX.2.121001

4. **Palacios, T., Rajan, S.** Use of Polarization-engineering to Improve AlGaN/GaN HEMTS *In: Advanced Semiconductor Materials and Devices Research: III-Nitrides and SiC* Edited by Cha, H.-Y. (Transworld Research Network, Kerala, India) 2009: pp. 175 – 202.

5. **Shen, L., Palacios, T., Poblenz, C., Corrion, A., Chakraborty, A., Fichtenbaum, N., Keller, S., Denbaars, S. P., Speck, J. S., Mishra, U. K.** Unpassivated High Power Deeply Recessed GaN HEMTs With Fluorine-Plasma Surface Treatment *IEEE Electron Device Letters* 27 (4) 2006: pp. 214 – 216.
   http://dx.doi.org/10.1109/LED.2006.871887

6. **Yu, H., Lisesivdin, S. B., Bolukbas, B., Kelekci, O., Ozturk, K. M. Ozcelik, S., Caliskan, D., Ozturk, M., Cakmak, H., Demirel, P, Ozbay, E.** Improvement of Breakdown Characteristics in AlGaN/GaN/$Al_xGa_{1-x}N$ HEMT Based on a Grading $Al_xGa_{1-x}N$ Buffer Layer *Physica Status Solidi A* 207 (11) 2010: pp. 2593 – 2596.
   http://dx.doi.org/10.1002/pssa.201026270

7. **Mochizuki, K., Terano, A., Kaneda, N., Mishima, T., Ishigaki, T., Tsuchiya, T.** Analysis of Leakage Current at Pd/AlGaN Schottky Barriers Formed on GaN Free-Standing Substrates *Applied Physics Express* 4 (2) 2011: p. 024104.
   http://dx.doi.org/10.1143/APEX.4.024104

8. **Singisetti, U., Wong, M. H., Speck, J. S., Mishra, U. K.** Enhancement-mode N-polar GaN MOS-HFET, with 5-nm GaN Channel, 510-mS/mm g_m, and and 0.66-Ω mm R_{on} *IEEE Electron Device Letters* 33 (1) 2012: pp. 26 – 28.
   http://dx.doi.org/10.1109/LED.2011.2170656

9. **Zhang, L., Wei, X. C., Liu, N. X., Lu, H. X., Zeng, J. P., Wang, J. X., Zeng, Y. P., Li, J. M**. Improvement of Efficiency of GaN-based Polarization-doped Light-emitting

Diodes Grown by Metal-organic Chemical Vapor Deposition *Applied Physics Letters* 98 (24) 2011: p. 241111.

10. **Wei, M. Wang, X., Pan, X., Xiao, H., Wang, C., Yang, C., Wang, Z.** Effect High Temperature AlGaN Buffer Thickness on GaN Epilayer Grown on Si(111) Substrates *Journal of Materials Science: Materials in Electronics* 22 2011: pp. 1028 – 1032.
http://dx.doi.org/10.1007/s10854-010-0254-0

11. **Yao, Ch., Yang, J., Pei-Qiang, X., Zi-Guang, M., Xiao-Li, W., Lu, W., Hai-Qiang, J., Hong, Ch.** Stress Control in GaN Grown on 6H-SiC by Metalorganic Chemical Vapor Deposition *Chinese Physics Letters* 28 (4) 2011: p. 048101.

12. **Grundmann M.** BandEng Alpha Version (2003); http://my.ece.ucsb.edu/mgrundmann/bandeng.htm.

13. **Juliano, P., Rosenbaum, E.** Accurate Wafer-level Measurement of ESD Protection Device Turn-on Using Modified Very Fast Transmission-line Pulse System *IEEE Transactions on Device and Materials Reliability* 1 (2) 2001: pp. 95 – 103.
http://dx.doi.org/10.1109/7298.956702

14. **Cha, H.-Y., Choi, Y. C., Eastman, L. F., Spencer, M. G., Ardaravičius, L., Matulionis, A., Kiprijanovič, O.** Influence of Low-field-mobility-related Issues on SiC Metal-semiconductor Field-effect Transistor Performance *Journal of Electronic Materials* 34 (4) 2005: pp. 330 – 335.
http://dx.doi.org/10.1007/s11664-005-0105-6

15. **Gaska, R., Osinsky, A., Yang, J. W., Shur, M. S.** Self-heating in High-power AlGaN/GaN HEMT's *IEEE Electron Device Letters* 19 (3) 1998: pp. 89 – 91.
http://dx.doi.org/10.1109/55.661174

16. **Bellotti, E., Bertazzi, F., Goano, M.** Alloy Scattering in AlGaN and InGaN: a Numerical Study *Journal of Applied Physics* 101 (12) 2007: p. 123706.

17. **Liberis, J., Ramonas, M., Kiprijanovič, O., Matulionis, A., Goel, N., Simon, J., Wang, K., Xing, H., Jena, D.** Hot Phonons in Si-doped GaN *Applied Physics Letters* 89 (20) 2006: p. 202117.
http://dx.doi.org/10.1063/1.2388866

18. **Ardaravičius, L., Ramonas, M., Kiprijanovič, O., Liberis, J., Matulionis, A., Eastman, L. F., Shealy, J. R., Chen, X., Sun, Y. J.** Comparative Analysis of Hot-electron Transport in AlGaN/GaN and AlGaN/AlN/GaN *Physica Status Solidi A* 202 (5) 2005: pp. 808 – 811.
http://dx.doi.org/10.1002/pssa.200461618

19. **Matulionis, A., Liberis, J., Matulionienė, I., Ramonas, M., Eastman, L. F., Shealy, J. R., Tilak, V., Vertiatchikh, A.** Hot-phonon Temperature and Lifetime in a Biased $Al_xGa_{1-x}N$/GaN Channel Estimated from Noise Analysis *Physical Review B* 68 (3) 2003: p. 035338.

20. **Tsen, K. T., Kiang, J. G., Ferry, D. K., Morkoc, H.** Subpicosecond Time-resolved Raman Studies of LO Phonons in GaN: Dependence on Photoexcited Carrier Density *Applied Physics Letters* 89 (11) 2006: p. 112111.
http://dx.doi.org/10.1063/1.2349315